JOURNAL OF GEOPHYSICAL RESEARCH, VOL. 99, NO. C5, PAGES 9785–9801, MAY 15, 1994

A three-scale composite surface model for the ocean wave–radar modulation transfer function

Roland Romeiser, Anke Schmidt, and Werner Alpers

Institut für Meereskunde, Universität Hamburg, Hamburg, Germany

Abstract. An improved three-scale composite surface model for the modulation of the radar backscatter from the ocean surface by long ocean waves is presented. The model is based on Bragg scattering theory. In the conventional two-scale model, only the geometric modulation of the radar backscatter and the hydrodynamic modulation of the short Bragg waves by the long waves is considered. In the three-scale model, the impact of intermediate-scale waves (wavelengths between the length of the Bragg waves and the length of the long waves which are resolved by the radar) is also taken into account, which leads to a modified theoretical ocean wave–radar modulation transfer function (MTF). For the first time the proposed model includes not only geometric effects associated with the intermediate-scale waves but also the additional hydrodynamic modulation of the Bragg waves. The resulting theoretical expression for the measured "hydrodynamic" MTF depends on the radar polarization as well as on the azimuthal (upwave / downwave or upwind / downwind) radar look direction. Especially for *HH* polarization, the predicted "hydrodynamic" MTF becomes significantly larger than expected from conventional theory. We compare model results with tower-based scatterometer measurements at *L*, *C*, and *X* band (1.0, 5.3, and 10.0 GHz, respectively), which were obtained during the Synthetic Aperture Radar and *X* Band Ocean Nonlinearities–Forschungsplattform Nordsee (SAXON-FPN) experiment. The measured magnitudes and phases of the MTF are better reproduced by the proposed three-scale model than by the conventional two-scale model. However, the large measured "hydrodynamic" MTFs for high microwave frequencies (*C* and *X* band) are still underestimated. The agreement between model predictions and measurements can be improved if, for example, an additional variation of the wind stress over the long waves is assumed. The required wind stress modulation depends on the long-wave slope and appears to be coupled to the hydrodynamic modulation of the surface roughness by a positive feedback mechanism.

1. Introduction

The ocean wave–radar modulation transfer function (MTF) describes the linear variations of the backscattered radar power from the ocean surface with the wave height or slope of long ocean waves [*Plant*, 1989]. Knowledge of the MTF is required, for example, when converting radar image intensity spectra of ocean scenes into ocean wave height spectra. Measurements of the MTF carried out from sea-based platforms under various environmental conditions have been reported by a number of authors since 1975 [*Keller and Wright*, 1975; *Alpers and Jones*, 1978; *Plant et al.*, 1978; *Wright et al.*, 1980; *Plant et al.*, 1983; *Feindt et al.*, 1986; *Schröter et al.*, 1986].

Paper number 93JC03372.
0148-0227/94/93JC-03372$05.00

An early theoretical description of the ocean wave–radar MTF was given by *Keller and Wright* [1975]. Based on Bragg scattering theory [*Wright*, 1968; *Valenzuela*, 1978], *Keller and Wright* [1975] separated the MTF into two parts, one describing the geometric modulation (tilt modulation) and the other describing the hydrodynamic modulation of the short Bragg waves by the orbital currents associated with the long waves. This concept is often referred to as the "two-scale model", since only the scales of the long waves and of the short Bragg waves are considered. Analytical expressions for the tilt MTF and the hydrodynamic MTF were given, for example, by *Alpers et al.* [1981] and by *Alpers and Hasselmann* [1978], respectively. However, it has been noted that this "conventional" theory underestimates the measured MTFs, in particular, at higher microwave frequencies (e.g., at 10 GHz (*X* band)) and at low wind speeds (say, 5 m/s). This was usually attributed to an underestimation of the hydrodynamic modulation [*Wright et al.*, 1980; *Schröter et al.*, 1986]. An additional modulation of the Bragg waves associated with the variation of the wind stress along the long waves has been hypothesized, for example, by *Alpers et al.* [1981], *Feindt* [1985], and *Hara and Plant* [this issue]. However, this effect would still be independent of the radar polarization and thus cannot explain a difference between the measured "hydrodynamic" MTFs for horizontal (HH) and vertical (VV) polarization, which has been clearly identified by W. Plant and others in data obtained in the framework of the Synthetic Aperture Radar and X Band Ocean Nonlinearities–Forschungsplattform Nordsee (SAXON-FPN) project.

A theoretical explanation for different "hydrodynamic" MTFs for HH and VV polarization was given by *Kasilingam and Shemdin* [1992], using a three-scale composite surface model. This model represents a combination of the conventional two-scale model and the composite surface model introduced by *Wright* [1968]. The three-scale concept was proposed first by *Lyzenga and Bennett* [1988] for the description of radar signatures of surface current variations over internal waves or underwater bottom topography. On the basis of Bragg scattering theory the composite surface model includes the impact of subresolution scale surface waves on the radar backscatter. In the three-scale model the spatial and temporal variations of these "intermediate-scale" waves are resolved. The resulting radar signatures of the long ocean waves show a more complex dependence on the radar polarization than expected from the two-scale model.

Kasilingam and Shemdin [1992] demonstrated that the description of the radar backscatter by the composite surface model is usually in good agreement with the results of a more general model based on the so-called Kirchhoff approximation of the Stratton-Chu integral [*Holliday et al.*, 1986, 1987]. The Stratton-Chu integral is the fundamental integral equation describing the interaction between an electromagnetic wave and a rough surface [*Stratton*, 1941]. Furthermore, *Kasilingam and Shemdin* [1992] showed that the ocean wave–radar modulation transfer functions obtained from the three-scale model and from conventional two-scale theory can differ significantly. However, their model results are based on the following simplifying assumptions:

(1) Only the hydrodynamic modulation of the intermediate-scale and short-wave spectrum by the long waves is taken into account. The asymmetric distribution of the Bragg waves along the intermediate-scale waves due to hydrodynamic modulation is neglected.

(2) In contrast to the composite surface model proposed by *Lyzenga and Bennett* [1988], *Kasilingam and Shemdin* [1992] assume that the sea surface is a perfect conductor. At VV polarization their approximation is valid for small (steep) incidence angles only. For larger incidence angles it leads to an underestimation of the tilt modulation of the backscattered power.

In this paper we present an improved three-scale composite surface model, which includes the effect of the two-scale hydrodynamic modulation of the Bragg waves. On the basis of a Taylor expansion of the backscattered radar power up to second order in the surface slope, the model is formulated in such a way that the impact of different modulation mechanisms is represented by separate terms. Model results are compared with data obtained from scatterometer measurements at the German Forschungsplattform Nordsee (Research Platform North Sea, FPN).

In section 2 the theory of the proposed model is described. An overview of the different contributions to the radar backscatter is given, and the linear modulation transfer function is defined. Furthermore, the modulation of ocean waves in a slowly varying surface current field according to weak hydrodynamic interaction theory is described.

General results of the proposed model are discussed in section 3. The composition of the theoretical MTF as a sum of the conventional components and the additional components arising from the three-scale model is illustrated. Model predictions are compared with experimental results in section 4, where the effect of an additional modulation of the wind stress over long waves is also investigated. A discussion of the results and an outlook are given in section 5.

2. Three-Scale Model

The basic concept of the three-scale composite surface model is illustrated in Figure 1. Waves of three different scales are treated separately in this model:

(1) The short "Bragg waves" give rise to resonant Bragg scattering of the radar signal. These waves experience a hydrodynamic modulation by all surface waves of longer wavelength.

(2) "Short intermediate-scale waves", that is, waves of wavelengths large compared to the Bragg wavelength, but smaller than the radar resolution cell ("subresolution scale waves"), cause a variation of the local surface elevation and incidence angle (geometric modulation),

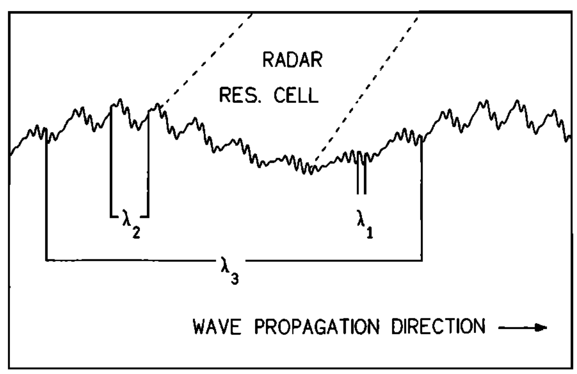

Figure 1. Schematic concept of the three-scale model. The three scales correspond to (1) the short Bragg waves of wavelength λ_1, (2) the intermediate-scale waves of wavelength λ_2, and (3) the long waves of wavelength λ_3. The intermediate-scale and Bragg waves are modulated hydrodynamically by the long waves, while the Bragg waves are also modulated by the intermediate-scale waves.

as well as a hydrodynamic modulation of the Bragg wave intensity within the radar resolution cell. These waves cannot be resolved by the radar, but their mean square slope, which is linearly related to the wave energy and thus subject to hydrodynamic modulation by the long waves, is not vanishing. The corresponding second-order terms of the backscattered power give a contribution to the radar signatures of the long waves and thus to the linear ocean wave–radar MTF. "Long intermediate-scale waves", that is, waves of wavelengths larger than the radar resolution cell but smaller than the long waves for which the ocean wave–radar MTF is evaluated, are resolved by the radar; that is, they modulate the backscattered power in space and time as they travel through the radar footprint. However, this modulation is not correlated with the long waves. Thus its linear component will average out. Again, only terms associated with the (hydrodynamically modulated) mean square slope of the intermediate-scale waves will survive when computing the ensemble average of the backscattered power distribution over several long-wave periods. Accordingly, short and long intermediate-scale waves give the same kind of contribution to the radar signatures of the long waves. The length of the radar resolution cell, which is the separating wavelength between long and short intermediate-scale waves, will therefore not enter into our theoretical considerations.

(3) The "long waves" are the waves for which the ocean wave–radar MTF is evaluated. Obviously, each harmonic long-wave component of the surface wave spectrum can give rise to hydrodynamic modulation of shorter waves only. Thus each long-wave component separates the wave spectrum into a short-wave part experiencing a "coherent" intensity modulation (the intermediate-scale and Bragg waves) and a long-wave part which does not vary in correlation with the profile of the harmonic long wave. The radar signatures of the long waves are due to variations of the surface elevation and slope, as well as to the hydrodynamic modulation of the Bragg waves and the intermediate-scale waves. In addition, the fact that the long waves also give a contribution to the mean square surface slope will lead to a slight modification of the mean backscattered radar power.

We shall confine the following discussion to a quasi-one-dimensional case in which the travel direction of all surface waves as well as the wind direction and the radar look direction are parallel to the x axis. This seems to be a reasonable approximation for the typical setup of scatterometer measurements from sea-based platforms, where data are taken only when the radar is looking against the waves (upwave).

2.1. Expansion of the Normalized Radar Cross Section

Besides the linear variations with the shape of a long wave, the radar backscatter from the ocean surface experiences a second-order modulation associated with quasi-random surface slope variations due to the other waves. In this section we develop the mathematical expressions describing the mean effect of this modulation. For this purpose we define the expectation value of a quantity G, $\langle G\rangle$, as ensemble average of the mean value of G over the radar resolution cell. This expectation value may be evaluated at a given phase position with respect to a particular long wave. It may vary in space and time along this wave. Thus $\langle G\rangle$ does not have to be equal to the total mean value of G. The variations of the expectation values of some quantities with respect to their mean values will enter into the definition of the ocean wave–radar MTF.

The backscattered radar power P from an illuminated area A_r at the sea surface, which could be a resolution cell within a radar image or the footprint of a scatterometer, is formally given by

$$P = \int_{A_r} dA\, \frac{\partial P}{\partial A} \qquad (1)$$

We assume that the integration is carried out over an area representing the projection of the actual surface onto a horizontal plane. According to basic electromagnetic and geometric principles, the portion of the backscattered power associated with an area element dA is given by

$$\frac{\partial P}{\partial A} = \frac{\alpha}{\langle r\rangle^4}\, w\, \sigma_0 \qquad (2)$$

where α is a proportionality factor depending on the total transmitted power, r is the distance between sea surface and radar antenna, w is a weighting function, and σ_0 is the normalized radar backscatter cross section per unit area (NRCS) of an illuminated facet. Here the weighting function w accounts for variations of the geometry and the radar power density at the illuminated facet with the local surface slope and elevation. For example, the projection onto the image plane is larger for surface facets which are tilted towards the antenna than for facets tilted away from the antenna. This variation of the geometric facet cross section with the variation of the local incidence angle of the radar is not included in the theoretical expression for σ_0. Also, the variations of the distance r and the corresponding variations of the illuminated area and the transmitted power density are included in w. The effects described by this weighting function will later be referred to as range and range-bunching modulation.

Neglecting spatial variations of the transmitted power density due to the antenna pattern, we obtain [compare *Plant*, 1989]

$$w = w(\zeta, s) = \frac{\langle H\rangle^2}{(\langle H\rangle - \zeta)^2}\, \frac{\cos(\langle\theta\rangle - s)}{\cos(\langle\theta\rangle)\cos(s)} \qquad (3)$$

Here θ and H denote the incidence angle of the radar and the vertical height of the antenna above the sea surface, respectively, ζ denotes the elevation of an illuminated facet with respect to the reference plane with incidence angle $\langle\theta\rangle$ and antenna height $\langle H\rangle$, and $s = \partial\zeta/\partial x$ denotes the corresponding (one-dimensional) facet slope. We define the "actual" normalized radar backscatter cross section of A_r, $\langle\sigma\rangle$, by

$$\langle P\rangle = A_r \frac{\alpha}{\langle r\rangle^4} \langle\sigma\rangle \tag{4}$$

Thus σ denotes the NRCS of a facet with respect to its projection onto the horizontal plane, while σ_0 denotes the NRCS with respect to the tilted facet itself. For moderate incidence angles (approximately 20° through 70°) the radar backscattering from the sea surface is dominated by resonant Bragg scattering. According to Bragg scattering theory [*Wright*, 1968; *Valenzuela*, 1978], the NRCS of a facet of the ocean is proportional to the (two-dimensional) wave height spectral density E of the resonant "Bragg" waves:

$$\sigma_0 = T(k_e, \theta)\, E(\underline{k}_B) \tag{5}$$

where

$$k_B = 2k_e \sin\theta \tag{6}$$

is the Bragg wavenumber and k_e is the electromagnetic wavenumber. The proportionality factor T can be found, for example, in the paper by *Valenzuela* [1978]. T depends on the polarization of the radar and on the relative dielectric constant of sea water, ϵ, which is a complex function of the frequency of the electromagnetic wave. Since the real part of ϵ is always large compared to 1 for microwaves [*Saxton and Lane*, 1952], the expressions for T given by *Valenzuela* [1978] can be approximated by

$$T_{HH} = 16\pi k_e^4 \cos^4\theta \tag{7a}$$

for horizontal (HH) polarization and

$$T_{VV} = 16\pi k_e^4 \cos^4\theta \left| \frac{\epsilon^2(1+\sin^2\theta)}{(\epsilon\,\cos\theta + \sqrt{\epsilon})^2} \right|^2 \tag{7b}$$

for vertical (VV) polarization.

The expectation value of the NRCS of the illuminated area, $\langle\sigma\rangle$, depends on the variability of s and ϵ on scales which are long compared to the Bragg wavelength. Furthermore, the long and intermediate-scale waves cause not only a geometric modulation of the local incidence angle and the distance between sea surface and radar antenna but also a hydrodynamic modulation of the Bragg waves, that is, of their wave height spectral density E. The hydrodynamic modulation may be written in terms of the surface slope as well. However, it depends on the wavenumber of the longer waves and must therefore be described in the wavenumber domain.

The instantaneous one-dimensional surface slope s at a position x within the illuminated area can be expressed by its Fourier transform $\hat{s}$:

$$s(x) = \int dk\, \hat{s}(k)\, e^{-ikx} \tag{8}$$

where $\hat{s}(-k) = \hat{s}^*(k)$. The corresponding expression for the square slope reads

$$s^2(x) = \iint dk_1\, dk_2\, \hat{s}(k_1)\, \hat{s}(k_2)\, e^{-i(k_1+k_2)x} \tag{9}$$

The NRCS can be decomposed into Fourier components as well. An expansion up to second order in s can formally be written as

$$\sigma(x) = \sigma_0(\langle\theta\rangle) + \int dk\, \hat{\sigma}(k)\, e^{-ikx} + \iint dk_1\, dk_2\, \hat{\hat{\sigma}}(k_1, k_2)\, e^{-i(k_1+k_2)x} \tag{10}$$

where we define $\hat{\sigma}(k)$ as the Fourier transform of the contributions to $\sigma(x)$, which depend linearly on the surface slope s, and $\hat{\hat{\sigma}}(k_1, k_2)$ as the Fourier transform of the contributions of second order in s. Although the variations of σ with a given wavenumber k depend to first order on the corresponding variations of s with the same wavenumber, the second-order components are associated with other waves: Components of s^2 with wavenumber k are obtained from each superposition of waves with wavenumbers k_1 and k_2 fulfilling the condition $k_1 + k_2 = k$. Thus (10) may also be written as

$$\begin{aligned}\sigma(x) &= \sigma_0(\langle\theta\rangle) + \int_{-k_{max}}^{+k_{max}} dk\, \hat{\sigma}(k)\, e^{-ikx} + \iint_{-k_{max}}^{+k_{max}} dk\, dk_2\, \hat{\hat{\sigma}}(k-k_2, k_2)\, e^{-ikx} \\ &= \sigma_0(\langle\theta\rangle) + \int_{-k_{max}}^{+k_{max}} dk \left(\hat{\sigma}(k) + \int_{-k_{max}}^{+k_{max}} dk_2\, \hat{\hat{\sigma}}(k-k_2, k_2) \right) e^{-ikx}\end{aligned} \tag{11}$$

Here the terms within the brackets represent the "complete" Fourier transform of σ, including all components up to second order in the surface slope. The maximum wavenumber of the variations of σ, k_{max}, is defined by the condition that the spatial scales of the surface slope modulating the Bragg scattering facets must be large compared to the Bragg wavelength. For our model simulations we choose a facet size of 6 times the Bragg wavelength, that is, $k_{max} = 1/6\, k_B$.

In terms of a Taylor expansion (11) reads explicitly

$$\begin{aligned}\sigma(x) = \sigma_0(\langle\theta\rangle) &+ \int_{-k_{max}}^{+k_{max}} dk\, \left.\frac{\partial\hat{\sigma}(k)}{\partial\hat{s}(k)}\right|_{\hat{s}=0} \hat{s}(k)\, e^{-ikx} \\ &+ \iint_{-k_{max}}^{+k_{max}} dk\, dk_2\, \frac{1}{2} \left.\frac{\partial^2\hat{\hat{\sigma}}(k-k_2, k_2)}{\partial\hat{s}(k-k_2)\partial\hat{s}(k_2)}\right|_{\hat{s}=0} \cdot \hat{s}(k-k_2)\, \hat{s}(k_2)\, e^{-ikx}\end{aligned} \tag{12}$$

When computing the expectation value $\langle\sigma\rangle$, the first integral vanishes, since the mean slope associated with the quasi-random waves must be zero. Thus we obtain

$$\langle\sigma\rangle = \sigma_0(\langle\theta\rangle) + \iint_{-k_{max}}^{+k_{max}} dk\, dk_2\, \frac{1}{2}\, \frac{\partial^2 \tilde{\sigma}}{\partial\hat{s}\partial\hat{s}}\bigg|_{\hat{s}=0} \langle \hat{s}(k-k_2)\,\hat{s}(k_2)\rangle\, e^{-ikx} \quad (13)$$

The expression containing the Fourier transforms of the wave slope is related to the (one-dimensional) wave height spectrum by

$$\langle \hat{s}(k-k_2)\,\hat{s}(k_2)\rangle = \frac{1}{2}\,\delta(k)\, k_2^2\, E(k_2) \quad (14)$$

Here the wave height spectrum $E(k)$ is defined in such a way that its integral over the positive k range yields the mean square surface elevation. Furthermore, δ denotes the Dirac delta distribution. Inserting (14) into (13) leads to

$$\langle\sigma\rangle = \sigma_0(\langle\theta\rangle) + \int_0^{k_{max}} dk\, \frac{1}{2}\, \mathrm{Re}\left(\frac{\partial^2\tilde{\sigma}(-k,k)}{\partial\hat{s}(-k)\partial\hat{s}(k)}\bigg|_{\hat{s}=0}\right) k^2\, E(k) \quad (15)$$

Inserting the expressions given by (2) and (5) into (1) and using the definition of σ given by (4), for the second derivative of $\tilde{\sigma}$ in (15) we obtain

$$\begin{aligned}
\frac{\partial^2\tilde{\sigma}}{\partial\hat{s}\partial\hat{s}}\bigg|_{\hat{s}=0} &= \frac{\partial^2\hat{T}}{\partial\hat{s}\partial\hat{s}}\bigg|_{\hat{s}=0} \Big\langle E(\underline{k}_B(\langle\theta\rangle))\Big\rangle \\
&+ 2\,\frac{\partial\hat{T}}{\partial\hat{s}}\bigg|_{\hat{s}=0} \frac{\partial\langle E\rangle}{\partial k}\bigg|_{\underline{k}=\underline{k}_B(\langle\theta\rangle)} \frac{\partial\hat{k}_B}{\partial\hat{s}}\bigg|_{\hat{s}=0} \\
&+ T(\langle\theta\rangle)\, \frac{\partial^2\langle E\rangle}{\partial k^2}\bigg|_{\underline{k}=\underline{k}_B(\langle\theta\rangle)} \left(\frac{\partial\hat{k}_B}{\partial\hat{s}}\bigg|_{\hat{s}=0}\right)^2 \\
&+ T(\langle\theta\rangle)\, \frac{\partial\langle E\rangle}{\partial k}\bigg|_{\underline{k}=\underline{k}_B(\langle\theta\rangle)} \frac{\partial^2\hat{k}_B}{\partial\hat{s}\partial\hat{s}}\bigg|_{\hat{s}=0} \\
&+ 2\,\frac{\partial\hat{T}}{\partial\hat{s}}\bigg|_{\hat{s}=0} \frac{\partial\hat{E}}{\partial\hat{s}}\bigg|_{\hat{s}=0} \\
&+ 2\,T(\langle\theta\rangle)\, \frac{\partial^2\hat{E}}{\partial k\partial\hat{s}}\bigg|_{\hat{s}=0,\,\underline{k}=\underline{k}_B(\langle\theta\rangle)} \frac{\partial\hat{k}_B}{\partial\hat{s}}\bigg|_{\hat{s}=0} \\
&+ T(\langle\theta\rangle)\, \frac{\partial^2\hat{E}}{\partial\hat{s}\partial\hat{s}}\bigg|_{\hat{s}=0} \\
&+ 2\,\frac{\partial\hat{w}}{\partial\hat{s}}\bigg|_{\hat{s}=0} \frac{\partial\hat{T}}{\partial\hat{s}}\bigg|_{\hat{s}=0} \Big\langle E(\underline{k}_B(\langle\theta\rangle))\Big\rangle \\
&+ 2\,\frac{\partial\hat{w}}{\partial\hat{s}}\bigg|_{\hat{s}=0} T(\langle\theta\rangle)\, \frac{\partial\langle E\rangle}{\partial k}\bigg|_{\underline{k}=\underline{k}_B(\langle\theta\rangle)} \frac{\partial\hat{k}_B}{\partial\hat{s}}\bigg|_{\hat{s}=0} \\
&+ 2\,\frac{\partial\hat{w}}{\partial\hat{s}}\bigg|_{\hat{s}=0} T(\langle\theta\rangle)\, \frac{\partial\hat{E}}{\partial\hat{s}}\bigg|_{\hat{s}=0} \\
&+ \frac{\partial^2\tilde{w}}{\partial\hat{s}^2}\bigg|_{\hat{s}=0} T(\langle\theta\rangle) \Big\langle E(\underline{k}_B(\langle\theta\rangle))\Big\rangle
\end{aligned} \quad (16)$$

Again, $\tilde{T}$, $\tilde{E}$, and $\tilde{w}$ denote Fourier transforms of the variations of T, E, and w of second order in the surface slope. Note the following:

(1) The variations of $\hat{T}$ and $\hat{k}_B$ with $\hat{s}$ are purely geometric, and T and k_B are always in phase or antiphase with s (depending on the azimuthal radar look direction). Thus the derivatives of the Fourier components of T and k_B with respect to those of s are independent of k and may be replaced by derivatives of the corresponding integrals, that is, by derivatives of T and k_B with respect to s.

(2) In contrast to other terms the hydrodynamic modulation, $\partial\hat{E}/\partial\hat{s}$, as well as the range-bunching modulation in $\partial\hat{w}/\partial\hat{s}$ are complex quantities. Only the real parts of the corresponding terms enter into the integral in (15).

For small slopes the relationship between the local surface slope s and the incidence angle θ can be approximated by

$$\theta = \langle\theta\rangle - \arctan(s) \approx \langle\theta\rangle - s \quad (17)$$

which implies

$$ds \approx -d\theta \quad (18)$$

Thus derivatives with respect to s may be replaced by derivatives with respect to θ. The hydrodynamic modulation of the Bragg waves by longer waves, $\partial\hat{E}/\partial\hat{s}$, can be parameterized by a complex hydrodynamic modulation transfer function [*Keller and Wright*, 1975; *Alpers and Hasselmann*, 1978; *Plant*, 1989]:

$$\frac{\partial\hat{E}}{\partial\hat{s}}\bigg|_{\hat{s}=0} = i\, M_h(\underline{k}, \underline{k}_B) \Big\langle E(\underline{k}_B(\langle\theta\rangle))\Big\rangle \quad (19)$$

Analytic expressions for M_h have been obtained, for example, by *Keller and Wright* [1975] and by *Alpers and Hasselmann* [1978]. For waves traveling in the positive x direction, M_h is given by

$$M_h = -\left(\frac{k_B}{\langle E(\underline{k}_B)\rangle} \frac{\partial\langle E\rangle}{\partial k}\bigg|_{\underline{k}=\underline{k}_B} - \gamma \right) \frac{\omega^2 + i\mu\omega}{\mu^2 + \omega^2} \quad (20)$$

Here ω denotes the angular frequency of the long wave (which, for reasons of consistency, must have the same sign as its wavenumber). Furthermore, γ denotes the ratio of the group velocity c_g and the phase velocity c_p of the Bragg waves, and μ denotes their relaxation rate (see section 2.3). Note that M_h depends on the frequency and thus on the wavenumber of the longer waves.

Inserting (16), (18), and (19) into (15) and separating the terms accounting for different modulation mechanisms, we finally obtain

$$\begin{aligned}\langle\sigma\rangle &= \sigma_0(\langle\theta\rangle) + \langle\sigma_{tt}\rangle + \langle\sigma_{th}\rangle + \langle\sigma_{hh}\rangle \\ &+ \langle\sigma_{rt}\rangle + \langle\sigma_{rh}\rangle + \langle\sigma_{rr}\rangle \end{aligned} \quad (21)$$

where

$$
\begin{aligned}
\langle\sigma_{tt}\rangle &= \langle\sigma_{tt}^{(1)}\rangle + \langle\sigma_{tt}^{(2)}\rangle + \langle\sigma_{tt}^{(3)}\rangle + \langle\sigma_{tt}^{(4)}\rangle \\
&= \frac{1}{2}\frac{\partial^2 T}{\partial\theta^2}\bigg|_{\langle\theta\rangle}\Big\langle E\big(\underline{k}_B(\langle\theta\rangle)\big)\Big\rangle\,\langle s^2\rangle \\
&\quad + \frac{\partial T}{\partial\theta}\bigg|_{\langle\theta\rangle}\frac{\partial\langle E\rangle}{\partial k}\bigg|_{\underline{k}_B(\langle\theta\rangle)}\frac{\partial k_B}{\partial\theta}\bigg|_{\langle\theta\rangle}\langle s^2\rangle \\
&\quad + \frac{1}{2}T(\langle\theta\rangle)\frac{\partial^2\langle E\rangle}{\partial k^2}\bigg|_{\underline{k}_B(\langle\theta\rangle)}\left(\frac{\partial k_B}{\partial\theta}\bigg|_{\langle\theta\rangle}\right)^2\langle s^2\rangle \\
&\quad + \frac{1}{2}T(\langle\theta\rangle)\frac{\partial\langle E\rangle}{\partial k}\bigg|_{\underline{k}_B(\langle\theta\rangle)}\frac{\partial^2 k_B}{\partial\theta^2}\bigg|_{\langle\theta\rangle}\langle s^2\rangle
\end{aligned}
\qquad (22)
$$

$$
\begin{aligned}
\langle\sigma_{th}\rangle &= \langle\sigma_{th}^{(1)}\rangle + \langle\sigma_{th}^{(2)}\rangle \\
&= \frac{\partial T}{\partial\theta}\bigg|_{\langle\theta\rangle}\Big\langle E\big(\underline{k}_B(\langle\theta\rangle)\big)\Big\rangle \\
&\quad\cdot\int_0^{k_{max}} dk\,\mathrm{Im}\Big(M_h\big(\underline{k},\underline{k}_B(\langle\theta\rangle)\big)\Big)\,k^2\,E(k) \\
&\quad + T(\langle\theta\rangle)\frac{\partial k_B}{\partial\theta}\bigg|_{\langle\theta\rangle} \\
&\quad\cdot\int_0^{k_{max}} dk\,\frac{\partial}{\partial k'}\Big(\mathrm{Im}\big(M_h(\underline{k},\underline{k}')\big)\big\langle E(\underline{k}')\big\rangle\Big)\bigg|_{\underline{k}_B(\langle\theta\rangle)}k^2\,E(k)
\end{aligned}
\qquad (23)
$$

$$
\langle\sigma_{hh}\rangle = \frac{1}{2}T(\langle\theta\rangle)\int_0^{k_{max}} dk\,\mathrm{Re}\left(\frac{\partial^2\hat{\hat{E}}}{\partial\hat{s}^2}\bigg|_{\hat{s}=0}\right)k^2\,E(k) \qquad (24)
$$

$$
\begin{aligned}
\langle\sigma_{rt}\rangle &= \langle\sigma_{rt}^{(1)}\rangle + \langle\sigma_{rt}^{(2)}\rangle \\
&= -\frac{\partial T}{\partial\theta}\bigg|_{\langle\theta\rangle}\Big\langle E\big(\underline{k}_B(\langle\theta\rangle)\big)\Big\rangle \\
&\qquad\cdot\int_0^{k_{max}} dk\,\mathrm{Re}\left(\frac{\partial\hat{w}}{\partial\hat{s}}\bigg|_{\hat{s}=0}\right)k^2\,E(k) \\
&\qquad - T(\langle\theta\rangle)\frac{\partial\langle E\rangle}{\partial k}\bigg|_{\underline{k}_B(\langle\theta\rangle)}\frac{\partial k_B}{\partial\theta}\bigg|_{\langle\theta\rangle} \\
&\qquad\cdot\int_0^{k_{max}} dk\,\mathrm{Re}\left(\frac{\partial\hat{w}}{\partial\hat{s}}\bigg|_{\hat{s}=0}\right)k^2\,E(k)
\end{aligned}
\qquad (25)
$$

$$
\begin{aligned}
\langle\sigma_{rh}\rangle &= \langle\sigma_{rh}^{(1)}\rangle + \langle\sigma_{rh}^{(2)}\rangle \\
&= -T(\langle\theta\rangle)\Big\langle E\big(\underline{k}_B(\langle\theta\rangle)\big)\Big\rangle \\
&\quad\cdot\int_0^{k_{max}} dk\,\mathrm{Re}\left(\frac{\partial\hat{w}}{\partial\hat{s}}\bigg|_{\hat{s}=0}\right)\mathrm{Im}\Big(M_h\big(\underline{k},\underline{k}_B(\langle\theta\rangle)\big)\Big)k^2 E(k) \\
&\quad - T(\langle\theta\rangle)\Big\langle E\big(\underline{k}_B(\langle\theta\rangle)\big)\Big\rangle \\
&\quad\cdot\int_0^{k_{max}} dk\,\mathrm{Im}\left(\frac{\partial\hat{w}}{\partial\hat{s}}\bigg|_{\hat{s}=0}\right)\mathrm{Re}\Big(M_h\big(\underline{k},\underline{k}_B(\langle\theta\rangle)\big)\Big)k^2 E(k)
\end{aligned}
\qquad (26)
$$

$$
\langle\sigma_{rr}\rangle = \frac{1}{2}\Big\langle E\big(\underline{k}_B(\langle\theta\rangle)\big)\Big\rangle\,T(\langle\theta\rangle)\cdot\int_0^{k_{max}} dk\,\mathrm{Re}\left(\frac{\partial^2\tilde{w}}{\partial\hat{s}^2}\bigg|_{\hat{s}=0}\right)k^2\,E(k) \qquad (27)
$$

Note that the components of $\langle\sigma_{tt}\rangle$ are directly proportional to the expectation value of the square slope of the sea surface, which is given by

$$
\langle s^2\rangle = \int_0^{k_{max}} dk\,k^2\,E(k) \qquad (28)
$$

The integrals in (23)–(27) are more complicated, since they include the hydrodynamic modulation transfer function M_h and derivatives of the weighting function w, which depend on k.

The derivatives of k_B are given explicitly by

$$
\frac{\partial k_B}{\partial\theta}\bigg|_{\langle\theta\rangle} = 2k_e\cos\langle\theta\rangle \qquad (29)
$$

$$
\frac{\partial^2 k_B}{\partial\theta^2}\bigg|_{\langle\theta\rangle} = -2k_e\sin\langle\theta\rangle \qquad (30)
$$

The derivatives of the weighting function w can be written explicitly as well. Formally, they must be written in terms of the Fourier transforms $\hat{w}$, $\tilde{w}$, and $\hat{s}$ because they are not independent of k. We obtain

$$
\frac{\partial\hat{w}}{\partial\hat{s}}\bigg|_{\hat{s}=0} = \tan\langle\theta\rangle - i\,\frac{2}{k\,\langle H\rangle} \qquad (31)
$$

$$
\frac{\partial^2\tilde{w}}{\partial\hat{s}^2}\bigg|_{\hat{s}=0} = \frac{6}{k^2\,\langle H\rangle^2} \qquad (32)
$$

The dependence of T on θ, and, in particular, the dependence of the wave height spectrum E on k, is unwieldy. Thus we compute the derivatives of T and E numerically.

The $\langle\sigma_{tt}\rangle$ terms represent the second-order tilt modulation of the NRCS by longer waves, while the $\langle\sigma_{th}\rangle$ terms are cross terms resulting from the correlation of tilt and hydrodynamic modulation. The term $\langle\sigma_{hh}\rangle$ represents the second-order hydrodynamic modulation of the Bragg waves. It will be neglected in the following, since no convincing theoretical description of this effect yet exists. An estimate of $\langle\sigma_{hh}\rangle$ can be found, for example, in the paper by *Plant* [1986], who concluded that this contribution is probably small. We shall show (see Figure 2) that, in most cases, at least the terms including first-order hydrodynamic modulation are small compared to the purely geometric terms. Similar to $\langle\sigma_{th}\rangle$, the terms of $\langle\sigma_{rt}\rangle$ and $\langle\sigma_{rh}\rangle$ are cross terms resulting from the correlation of the range and range-bunching modulation with the tilt modulation and the hydrodynamic modulation, respectively. The last term, $\langle\sigma_{rr}\rangle$, describes second-order range modulation; that is, it accounts for the fact that the increase of the contribution of facets with positive elevation to the mean NRCS is larger than the corresponding decrease of the contribution of facets with negative elevation. This term, as well as $\langle\sigma_{rh}^{(2)}\rangle$, decreases with increasing distance between the radar antenna and the sea surface. For distances larger than, say, 100 m, both contributions are negligible.

A notable fact is that $\langle\sigma_{th}\rangle$ and $\langle\sigma_{rh}^{(1)}\rangle$ change sign when the azimuthal radar look direction is reversed, since the maximum intensity of the Bragg waves is always located at the same side of the long waves (which is, according to weak hydrodynamic interaction theory, the forward face). In contrast to this the sign of all other terms remains the same. Thus the proposed model predicts an upwave / downwave asymmetry of the NRCS (see also *Plant* [1986]). We define $\langle\sigma_2^{(s)}\rangle$ and $\langle\sigma_2^{(a)}\rangle$ as sums of the symmetric and the asymmetric components of $\langle\sigma\rangle$, respectively:

$$\langle\sigma_2^{(s)}\rangle = \langle\sigma_{tt}\rangle + \langle\sigma_{rt}\rangle + \langle\sigma_{rh}^{(2)}\rangle \tag{33}$$

$$\langle\sigma_2^{(a)}\rangle = \langle\sigma_{th}\rangle + \langle\sigma_{rh}^{(1)}\rangle \tag{34}$$

The dependence of $\langle\sigma_2^{(s)}\rangle$ and $\langle\sigma_2^{(a)}\rangle$ on θ is shown in Figure 2 for the radar frequencies 1 GHz (*L* band) and 10 GHz (*X* band) at both *HH* and *VV* polarization. Note that the second-order terms of $\langle\sigma\rangle$ are much larger at *X* band than at *L* band. Furthermore, the asymmetric terms, which are a new feature of the pro-

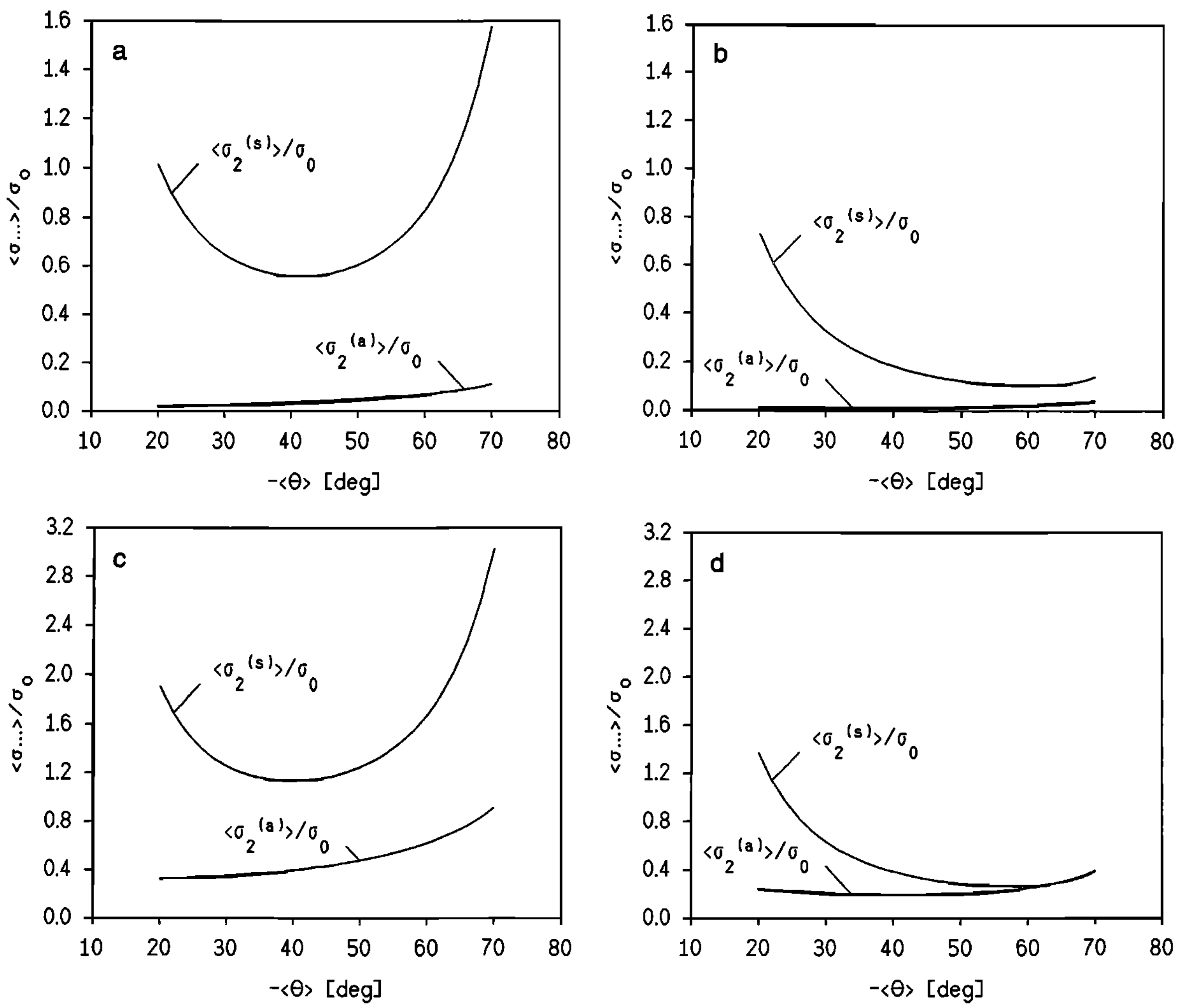

Figure 2. Relative contributions of the "symmetric" and "asymmetric" second-order terms of the NRCS as given by (33) and (34) to the total NRCS, normalized by $\sigma_0(\langle\theta\rangle)$. The "asymmetric" terms change sign when the azimuthal radar look direction is reversed. The wind speed is 10 m/s, the radar look direction is upwave, the height of the radar antenna above the sea surface is 26 m. (a) *L* band, *HH* polarization. (b) *L* band, *VV* polarization. (c) *X* band, *HH* polarization. (d) *X* band, *VV* polarization.

posed model, give a considerably large contribution at X band (Figures 2c and 2d). At VV polarization this becomes the dominant second-order contribution for incidence angles larger than approximately 55°. Thus the impact of the hydrodynamic modulation is not negligible at high microwave frequencies.

So far we have considered only the expectation value $\langle\sigma\rangle$ of the NRCS for an illuminated area with the nominal incidence angle $\langle\theta\rangle$, which could be located at a certain phase position with respect to a long wave. We now want to analyze the linear spatial and temporal variation of this expectation value along the long waves. These large-scale variations of the NRCS can be written as a Taylor series up to first order in the long-wave slope $S(x)$. If $\widehat{S}(K)$ denotes the Fourier transform of $S(x)$ and Ω denotes the long-wave angular frequency, we obtain

$$\begin{aligned}\langle\sigma\rangle(x,t) &= \overline{\sigma_0} + \overline{\langle\sigma_2^{(s)} + \sigma_2^{(a)}\rangle} \\ &+ \int_{-K_{cut}}^{+K_{cut}} dK\, \frac{\partial\widehat{\sigma}_0}{\partial\widehat{S}}\, \widehat{S}(K)\, e^{-i(Kx-\Omega t)} \\ &+ \int_{-K_{cut}}^{+K_{cut}} dK\, \frac{\partial}{\partial\widehat{S}} \left(\widehat{\langle\sigma_2^{(s)}\rangle} + \widehat{\langle\sigma_2^{(a)}\rangle}\right) \widehat{S}(K) e^{-i(Kx-\Omega t)}\end{aligned} \tag{35}$$

Here the bar denotes averaging in space and time over the long waves. The cutoff wavenumber, K_{cut}, is the maximum wavenumber which is resolved by the radar. In the case of a scatterometer this quantity depends on the size of the radar footprint.

Note that the hydrodynamic modulation caused by a particular long wave of wavenumber K can affect only the waves of wavenumbers larger than K. Thus the modulation of the second-order terms of $\langle\sigma\rangle$ by a long wave of wavenumber K depends on the contribution of the integration interval between K and K_{cut} to the integrals in (23)–(28).

2.2. Linear Modulation Transfer Function

The modulation of the backscattered radar intensity by long ocean waves can be described, to a good approximation, by a linear relationship [*Keller and Wright*, 1975; *Alpers and Hasselmann*, 1978; *Alpers et al.*, 1981; *Plant*, 1989]. The (one-dimensional) complex ocean wave–radar modulation transfer function (MTF) is defined by

$$M(K) = -i\, \frac{1}{\overline{\langle P\rangle}}\, \frac{\partial\widehat{\langle P\rangle}(K)}{\partial\widehat{S}(K)}\bigg|_{\widehat{S}=0} \tag{36}$$

Here the phase of the MTF is defined in such a way that a phase of 0 means that maximum backscattered power occurs at the wave crest and a positive phase means that it occurs at the forward face of the wave. Using (36), the variations of the backscattered power which are linear in the long-wave slope can be written as

$$\langle P\rangle(x,t) = \overline{\langle P\rangle} \left(1 + \int_{-K_{cut}}^{+K_{cut}} dK\, i\, M(K) \widehat{S}(K) e^{-i(Kx-\Omega t)}\right) \tag{37}$$

The relationship between the backscattered power and $\langle\sigma\rangle$ was given by (4). The conventional expression for the MTF, which is obtained in the two-scale theory under the assumption that $\langle\sigma\rangle = \sigma_0(\langle\theta\rangle)$, is usually written as the sum of three terms describing range, tilt, and hydrodynamic modulation:

$$M = M_R + M_T + M_H \tag{38}$$

The "range MTF", M_R, describes the modulation of the backscattered power due to geometric modulation of the illuminated patch at the sea surface. It is given by

$$M_R = -i\, \frac{\overline{\langle r\rangle^4}}{\overline{A_r}}\, \frac{\partial}{\partial\widehat{S}}\, \frac{\widehat{A}_r}{\langle r\rangle^4} \tag{39}$$

If only the modulation of the distance between the radar antenna and the illuminated patch is taken into account, one obtains for a continuous wave (CW), "beam-limited" scatterometer (see *Plant* [1989])

$$M_R^{(rg)} = \frac{2}{KH_0} \tag{40}$$

where H_0 denotes the "nominal"(mean) height of the radar antenna above the sea surface. For radar measurements carried out from airborne or spaceborne systems, $M_R^{(rg)}$ is usually negligible, while it may contribute considerably to the MTF measured by scatterometer from sea-based platforms.

Another term contributing to the ocean wave–radar MTF was discussed by *Gower* [1983]. It is associated with the modulation of the size of the illuminated area A_r due to the slope of the sea surface. For a CW, "beam-limited" scatterometer, this "range-bunching MTF" is given by [see *Plant*, 1989]

$$M_R^{(rb)} = i\tan\theta_0 \tag{41}$$

where θ_0 denotes the "nominal"(mean) incidence angle.

The "tilt MTF", M_T, describes the geometric modulation of σ_0 by the long waves. The conventional theoretical expression for the tilt MTF [e.g., *Alpers et al.*, 1981] reads

$$M_T^{(0)} = i\, \frac{1}{\sigma_0} \left(\frac{\partial T}{\partial\theta}\bigg|_{\theta_0} E_0(\underline{k}_{B0}) + T(\theta_0)\frac{\partial E}{\partial k}\bigg|_{\underline{k}_{B0}} \frac{\partial k_B}{\partial\theta}\bigg|_{\theta_0}\right) \tag{42}$$

Here k_{B0} denotes the "nominal" value of k_B, which is equal to the mean value of $k_B(\langle\theta\rangle)$ as used before, and E_0 denotes the equilibrium wave height spectrum. Figure 3 shows $M_T^{(0)}$ for X band as function of θ for HH and VV polarization. Here the dielectric constant ϵ as given by *Saxton and Lane* [1952] was used. In addition, the tilt MTF for VV polarization and a perfectly conduct-

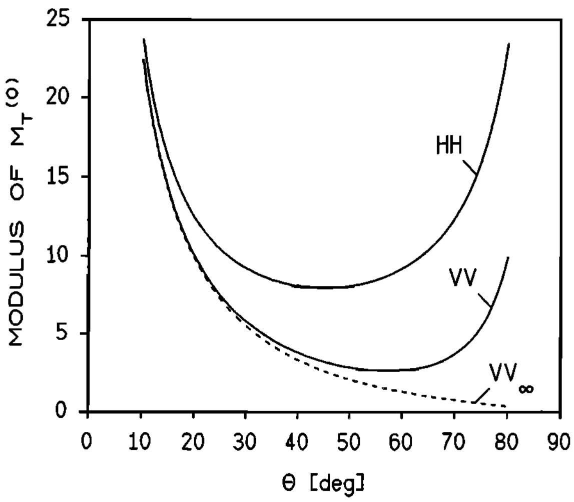

Figure 3. Tilt modulation transfer function $M_T^{(0)}$ for the polarizations *HH* and *VV*, as given by (42). The solid line represents the tilt MTF obtained for the dielectric constant ϵ for *X* band; the dashed line represents an approximation for a perfectly conducting surface ($\epsilon \rightarrow \infty$).

ing surface ($\epsilon \rightarrow \infty$) is shown in Figure 3. Obviously this approximation is valid only for small incidence angles up to approximately 30°.

The "hydrodynamic MTF", M_H, describes the variation of the Bragg wave energy along the long waves due to hydrodynamic modulation, that is, the deviation of the wave height spectral density of the Bragg waves from its equilibrium value. The conventional hydrodynamic MTF is defined as

$$M_H^{(0)} = -i \, \frac{1}{E_0} \, \frac{\partial \widehat{E}}{\partial \widehat{S}} \bigg|_{\widehat{S}=0} \tag{43}$$

An analytic solution obtained from weak hydrodynamic interaction theory was given already by (20). In terms of the "long" waves (switching again to capital letters for variables associated with the long wave), it reads

$$M_H^{(0)} = - \left(\frac{k_B}{E_0(\underline{k}_B)} \, \frac{\partial E_0}{\partial k} \bigg|_{\underline{k}=\underline{k}_{B0}} - \gamma \right) \frac{\Omega^2 + i\mu\Omega}{\mu^2 + \Omega^2} \tag{44}$$

In the three-scale model the mean value of the NRCS is the mean value of $\langle\sigma\rangle$ instead of $\sigma_0(\theta_0)$ (see (21)). The corresponding increase of the mean backscattered power leads to a reduction of the MTF, which can be included in the model by introducing the additional components

$$M_T^{(1)} = \left(\frac{\sigma_0}{\langle\sigma\rangle} - 1 \right) M_T^{(0)} \tag{45}$$

and

$$M_H^{(1)} = \left(\frac{\sigma_0}{\langle\sigma\rangle} - 1 \right) M_H^{(0)} \tag{46}$$

as "correction terms" for M_T and M_H, respectively. Note that $M_T^{(1)}$ and $M_H^{(1)}$ describe the first-order modulation of the backscattered radar power by the long waves in the same way as the conventional components $M_T^{(0)}$ and $M_H^{(0)}$. The superscript numbers and letters represent only indices which do not correspond to the order of the terms.

In addition, the modulation of the second-order terms of $\langle\sigma\rangle$ by the long waves must be taken into account. These terms experience a tilt modulation with the modulation of $\langle\theta\rangle$, as well as a hydrodynamic modulation of the Bragg waves and the intermediate-scale waves by the long waves. We define

$$M_2^{(s)} = -i \, \frac{1}{\langle\sigma\rangle} \, \frac{\partial}{\partial \widehat{S}} \widehat{\left\langle \sigma_2^{(s)} \right\rangle} \tag{47}$$

$$M_2^{(a)} = -i \, \frac{1}{\langle\sigma\rangle} \, \frac{\partial}{\partial \widehat{S}} \widehat{\left\langle \sigma_2^{(a)} \right\rangle} \tag{48}$$

where $M_2^{(s)}$ accounts for the modulation of the second-order terms which are symmetric with respect to the azimuthal radar look direction and $M_2^{(a)}$ accounts for the modulation of the asymmetric second-order terms.

In addition to the pure hydrodynamic modulation discussed so far, a variation of the wind stress along the long waves might give rise to an additional modulation of the intermediate-scale and Bragg waves. Formally, a "wind MTF", M_W, may be introduced, which accounts for this effect. The magnitude of M_W can be roughly estimated by comparing measured MTFs with theoretical results. Of course, one has to keep in mind that remaining discrepancies could also be due to other modulation mechanisms.

2.3. Hydrodynamic Modulation

Assuming that the scales of a short Bragg wave or intermediate-scale wave in space and time are small compared to the scales of the surface current field caused by the long waves, the current–wave interaction can be described by a Wentzel-Kramers-Brillouin (WKB) type theory [*Schiff*, 1955; *Longuet-Higgins and Stewart*, 1964; *Whitham*, 1965; *Bretherton*, 1970; *Willebrand*, 1975; *Alpers and Hasselmann*, 1978; *Alpers and Hennings*, 1984]. According to this "weak hydrodynamic interaction" theory, wave packets traveling through a slowly varying current field along given trajectories obey the action balance equation

$$\frac{dN}{dt} = \left(\frac{\partial}{\partial t} + \frac{d\underline{x}}{dt} \frac{\partial}{\partial \underline{x}} + \frac{d\underline{k}}{dt} \frac{\partial}{\partial \underline{k}} \right) N = Q(\underline{k}, \underline{x}, t) \tag{49}$$

Here N denotes the action density of a surface wave packet, which is proportional to the spectral energy density E times the intrinsic phase speed of the short waves. The source function Q describes the combined effect of wind input, wave–wave interaction, and dissipation, which forces the spectrum to return to equilibrium after experiencing a perturbation. For small perturbations the source function can be approximated by a linear diagonal operator of the form

$$Q = -\mu \, \delta N \tag{50}$$

where

$$\delta N = N(\underline{k}, \underline{x}, t) - N_0(\underline{k}) \quad (51)$$

is the deviation of the action density from its equilibrium value N_0 and μ is the so-called relaxation rate [*Miles*, 1959; *Snyder and Cox*, 1966; *Inoue*, 1967; *Keller and Wright*, 1975; *Hughes*, 1978; *Wright*, 1978; *Alpers and Hasselmann*, 1978; *Snyder et al.*, 1981; *Mitsuyasu and Honda*, 1982; *Plant*, 1982; *Alpers and Hennings*, 1984]. The different parameterizations of μ used by these authors differ by up to one order of magnitude [*Caponi et al.*, 1988]. Thus the relaxation rate is, to some extent, a weak element of our theory. For the model simulations presented in this paper we have chosen the parameterization given by *Hughes* [1978]. Figure 4 shows μ as function of wavenumber k for the wind speeds of 5, 10, and 15 m/s.

An analytic expression for the hydrodynamic modulation is represented by the hydrodynamic MTF as given by (20) and (44). It is applicable to the modulation of short Bragg waves as well as to the modulation of the intermediate-scale waves by the long waves. According to this solution, the maximum intensity of the short ripple waves with large relaxation rates should be found at phases close to 90° ahead of the long-wave crest, that is, at the forward face of the wave, where the maximum convergence of the surface current field occurs. The weak relaxation of the longer intermediate-scale waves leads to an integration of the hydrodynamic modulation over longer distances, yielding the largest intensity of these waves close to the end of convergent current regions. This corresponds to phase positions close to the long-wave crest.

In principle, the analytical solution of the action balance equation could be used for computing the hydrodynamic modulation of the entire intermediate-scale and short wave spectrum. However, it is used in our simulations only for modeling the hydrodynamic modulation of the Bragg waves by the intermediate-scale waves. For the computation of the modulated intermediate-scale wave spectra, the action balance equation is integrated numerically, which allows an easy introduction of a wind stress modulation over the long waves (see section 4.2), or of other modulation mechanisms. A variable wind stress affects the relaxation rate μ as well as the equilibrium wave height spectrum.

For the equilibrium spectrum we choose a parameterization similar to the one given by *Bjerkaas and Riedel* [1979], which is a combination of five wave spectra defined for different wavenumber ranges. The Bjerkaas-Riedel spectrum has already been used successfully for similar model calculations by D. Thompson and coworkers [*Thompson and Gasparovic*, 1986; *Thompson*, 1989, 1990; *Thompson et al.*, 1991]. The slope spectrum for wind speeds of 5, 10, and 15 m/s is shown in Figure 5.

3. General Characteristics of the Model

We now want to discuss the general differences between the MTF obtained from the proposed three-scale model and from conventional theory. For this purpose we have computed the variation of the radar backscatter along a 100 m wave for L and X band (1.0 and 10.0 GHz, respectively), HH and VV polarization, and for a wind speed of 10 m/s. The nominal incidence angle of the radar is 45°, looking upwave, and the height of the antenna above the sea surface is 26 m. The resulting MTFs are shown in the diagrams in Figure 6.

The four diagrams in the top row of Figures 6a-6d show the different components of the MTF for the four radar channels considered here as complex vector sums. In the second row the resulting total MTFs as given by conventional theory and by the proposed three-scale model are shown. Finally, the bottom row of diagrams shows the "residual" modulation transfer function M_{RES}, which we define as the difference between the total MTF and the conventional geometric MTF consisting of M_R and $M_T^{(0)}$, that is,

$$\begin{aligned} M_{RES} &= M - M_R - M_T^{(0)} \\ &= M_H^{(0)} + M_T^{(1)} + M_H^{(1)} + M_2^{(s)} + M_2^{(a)} \end{aligned} \quad (52)$$

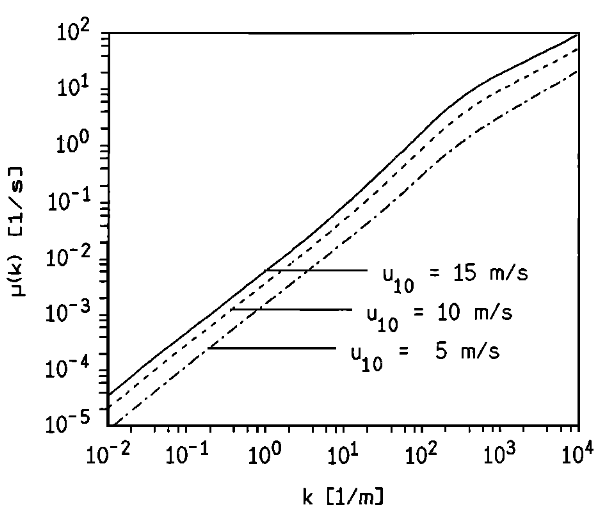

Figure 4. Relaxation rate $\mu(k)$ for wind speeds of 5, 10, and 15 m/s, as given by *Hughes* [1978].

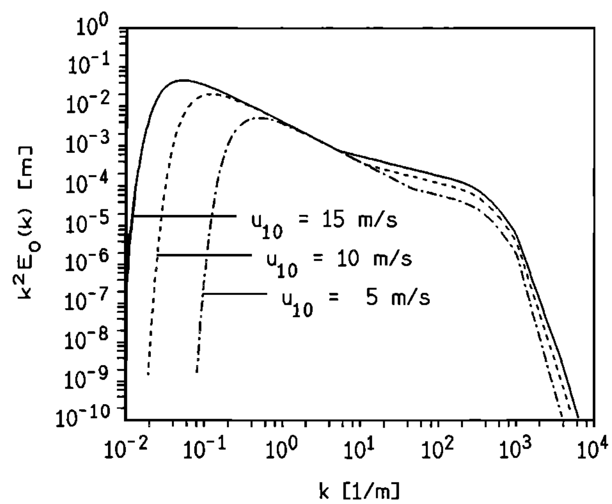

Figure 5. Slope spectrum of ocean waves for wind speeds of 5, 10, and 15 m/s, as given by *Bjerkaas and Riedel* [1979].

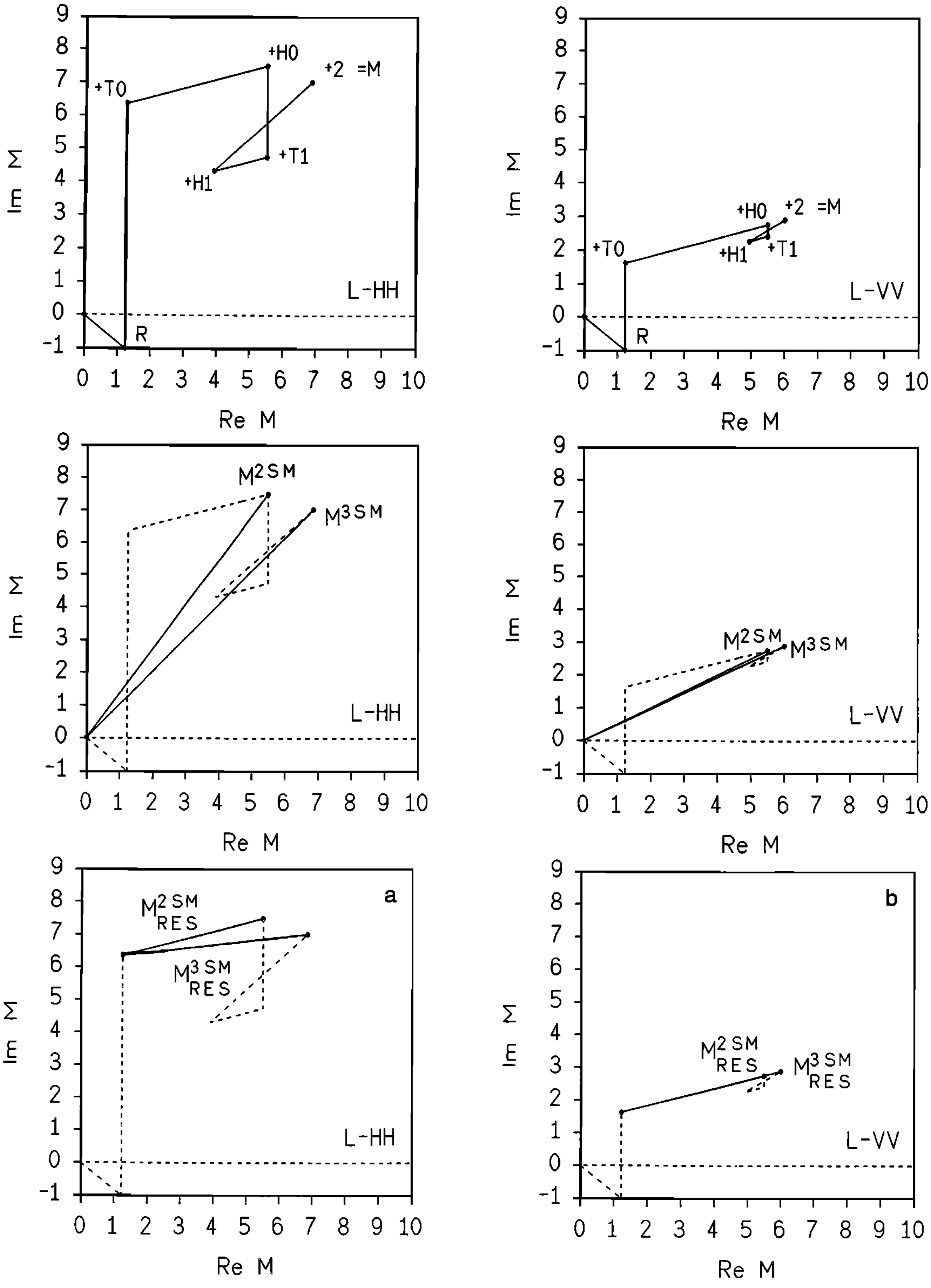

Figure 6. Composition of the real and the imaginary part of the total MTF according to the proposed three-scale model for a 100 m wave. The wind speed is 10 m/s, the incidence angle is 45°, the azimuthal radar look direction is upwave, the height of the radar antenna above the sea surface is 26 m. (a) L band, HH polarization. (b) L band, VV polarization. (c) X band, HH polarization. (d) X band, VV polarization. (top) Vector sums of the different components. (center) Resulting total MTFs. (bottom) Resulting "residual" MTFs as defined by (52). Legend: T0, $M_T^{(0)}$; etc.; 2SM, two-scale (conventional) model; 3SM, proposed three-scale model.

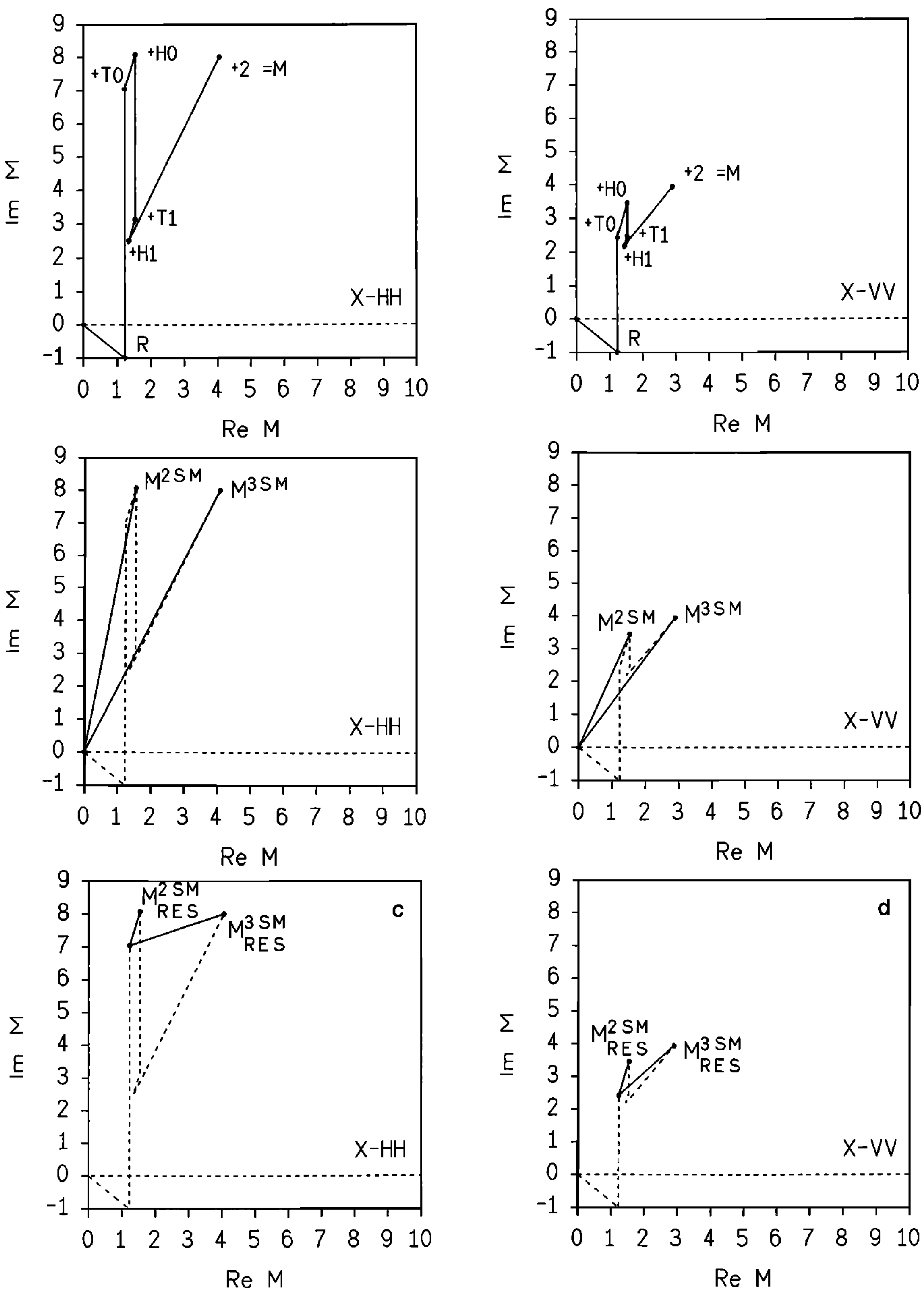

Figure 6. (continued).

According to conventional theory the "residual" MTF should be equal to the hydrodynamic modulation transfer function $M_H^{(0)}$, which is independent of the radar polarization. Figure 6 shows that particularly at X band the three-scale model predicts a pronounced difference between the "residual" MTFs for HH and VV polarization, yielding a larger modulus for HH polarization. The phases of the total MTF are generally shifted backwards, that is, against the wave travel direction, when switching from the conventional model to the proposed model.

4. Comparison of Model Results With Measurements

Since the conventional tilt modulation transfer function $M_T^{(0)}$ can easily be calculated from Bragg scattering theory, it has been common practice in literature [*Wright et al.*, 1980; *Schröter et al.*, 1986] to subtract it, together with the range MTF, M_R, from the measured total MTF, expecting to obtain the hydrodynamic MTF as a residual component for further analysis. We shall keep this method here in order to obtain comparable results, that is, we shall compare measured and theoretical values of the "residual" modulation transfer function M_{RES} as given by (52).

We carried out extensive MTF measurements from the German "Forschungsplattform Nordsee" (North Sea Research Platform or FPN) within the framework of the SAXON-FPN project. Data were obtained from a three-frequency (L, C, and X band), dual-polarization (HH and VV) Doppler scatterometer. The incidence angle of the system was 45°, the height of the antenna above the mean sea level was 26 m, and the length of the illuminated patch in the radar look direction was 15 m at L band (1.0 GHz), 2.9 m at C band (5.3 GHz), and 1.5 m at X band (10.0 GHz). The intensity and the Doppler shift of the backscattered radar signal were measured simultaneously. Since the Doppler shift can be converted into long-wave slope by a linear transformation [*Feindt et al.*, 1986] (which is still a reasonable assumption within the three-scale theory), MTFs could be determined this way without using additional data from other sources. The data considered here are some results obtained from measurements performed between March and November 1992. A more detailed presentation of our experimental results will be given in another paper.

"Residual" MTFs have been computed for the wind speed intervals of 3-6 and 14-16 m/s, which we refer to as data for 5 and 15 m/s, respectively. Only upwind and upwave cases are considered, that is, cases in which the wind and wave directions were "from west" within an interval of ±30°, while the radar antenna was pointing due west. The MTFs have been averaged over several measurements obtained at different sea states. Furthermore, only data points associated with a squared coherence between the wave slope and the backscattered power of better than 0.4 have been taken into account, since the linear MTF theory is useful only in cases of a basically linear relationship between the two quantities.

4.1. Simulations Without Wind Modulation

Magnitudes and phases of measured "residual" MTFs for wind speeds of 15 and 5 m/s are shown together with theoretical values in Figures 7 and 8, respectively. While the dashed lines represent the conventional hydrodynamic modulation transfer function $M_H^{(0)}$ as given by (44), the solid lines denote M_{RES} as obtained from the proposed three-scale model. Since the scatterometer measurements were obtained as time series, the MTFs

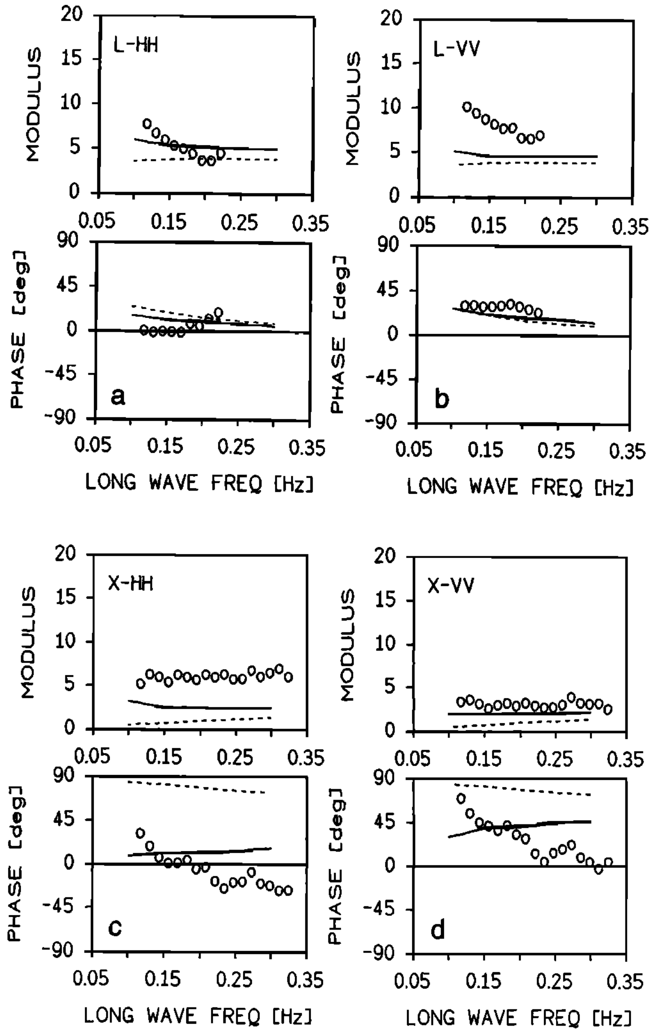

Figure 7. "Residual" MTFs for a wind speed of 15 m/s. (a) L band, HH polarization. (b) L band, VV polarization. (c) X band, HH polarization. (d) X band, VV polarization. The circles represent experimental results, the dashed lines represent the conventional hydrodynamic MTF, the solid lines represent M_{RES} as obtained from the three-scale model.

are shown as functions of the long-wave frequency. A typical peak frequency encountered during our measurements is 0.15 Hz, which corresponds to a wavelength of approximately 70 m.

However, the plots indicate that the dependence of the measured as well as the theoretical "residual" MTFs on the long-wave frequency is relatively weak in most cases. A notable increase of the measured modulus of M_{RES} at low wave frequencies is found only at L band (Figures 7a and 7b), which is reproduced neither by the conventional two-scale nor by the proposed three-scale model. The "residual" MTFs for L band are almost independent of wind speed. The differences between the magnitudes of the "residual" MTFs obtained from the three-scale model and from the conventional model are relatively small. Besides the underestimation of M_{RES} at lower wave frequencies, the L band model results show reasonable agreement with the data.

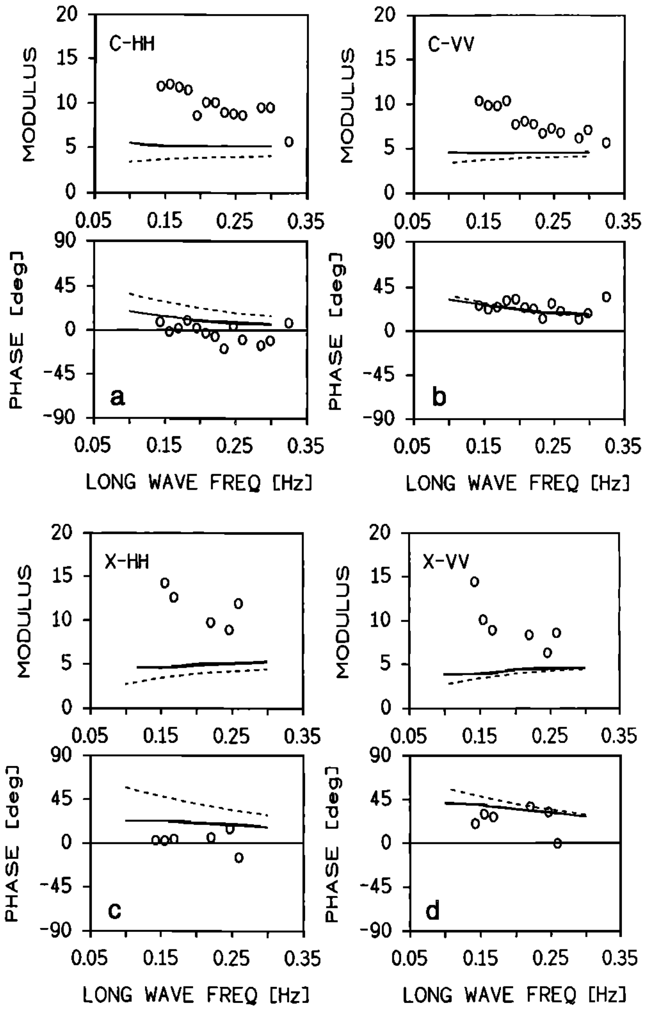

Figure 8. Same as Figure 7, but for a wind speed of 5 m/s. (a) L band, HH polarization. (b) L band, VV polarization. (c) X band, HH polarization. (d) X band, VV polarization.

The "residual" MTFs for X band at 15 m/s are shown in Figures 7c and 7d. The measured MTFs show a pronounced difference between HH and VV polarization, where a larger magnitude and a slightly negative phase is obtained at HH polarization. This behavior is qualitatively reproduced by the three-scale model. However, the differences are much less pronounced: While the measured "residual" MTF seems to be approximately 2 times larger for HH than for VV polarization, the corresponding ratio obtained from the proposed model is still close to 1. The theoretical modulus of M_{RES} for HH polarization appears to be clearly underestimated, although the modulus obtained from the three-scale model already exceeds the modulus of the conventional hydrodynamic MTF by a factor of more than 2. The measured phases of M_{RES} for HH and VV polarization are reproduced relatively well by the proposed model, whereas the phases of $M_H^{(0)}$ exceed the measured values by up to 90° or more.

Figure 8 shows the "residual" MTFs for C and X band at a wind speed of 5 m/s. Basically the measured MTFs for both frequencies are similar: Their magnitudes are strongly increased with respect to the 15 m/s case (not shown for C band), and only small differences between M_{RES} for HH and VV polarization are found. Also the difference between the measured phases of M_{RES} for HH and VV polarization decreases with decreasing wind speed. Again, the phases of M_{RES} as obtained from the three-scale model show good agreement with the data, while the large magnitudes are not reproduced satisfactorily. It seems to be essential to consider additional modulation mechanisms in order to explain the large measured modulation.

4.2. Simulations Including Wind Modulation

It has been hypothesized by several authors [e.g., *Wright et al.*, 1980; *Schröter et al.*, 1986; *Hara and Plant*, this issue] that a modulation of the friction velocity u_* of the wind field over long waves leads to an increased modulation of the shorter waves, which could explain the large measured "hydrodynamic" or "residual" MTFs for high microwave frequencies. This mechanism seems to be the most promising one for the explanation of the large measured modulation for C and X band at low and moderate wind speeds (say, 5 m/s). Its impact on the results of the three-scale model will be discussed in this section. Since a modulation of the wind stress affects the components of the MTF in different ways, additional numerical simulations had to be carried out.

A theoretical description of the different source terms describing the response of the wave spectrum to changes of the friction velocity was given by *Smith* [1990]. However, this theory is quite unwieldy and includes several parameters which are not well known. Therefore the following theoretical considerations are still based on the simplified action balance equation with a linear source function as given by (49)–(51).

Measurements of the wind stress modulation over long waves in the vicinity of FPN have been carried out by *Stolte* [1984, 1991], using fixed tower-based anemometers as well as anemometers carried by a specially developed drift buoy. The intensity as well as the phase of the friction velocity modulation show a great deal of scatter and seem to depend on sea state as well as on wind speed. Therefore we introduce a sinusoidal wind stress modulation and consider its amplitude and phase as free parameters. These parameters may be tuned in such a way that the best agreement between the theoretical and the measured ocean wave–radar MTF is obtained. We define the wind stress modulation transfer function by

$$\frac{\widehat{\langle u_* \rangle}(K)}{\langle u_* \rangle} = i\,M_{u_*}(K)\,\widehat{S}(K) \tag{53}$$

The friction velocity u_* enters into the relaxation rate μ as well as into the local equilibrium wave height spectrum. Figure 9 shows how μ and E_0 as given by *Hughes* [1978] and by *Bjerkaas and Riedel* [1979], respectively, vary with deviations of u_* from its mean value at a wind speed of 5 m/s.

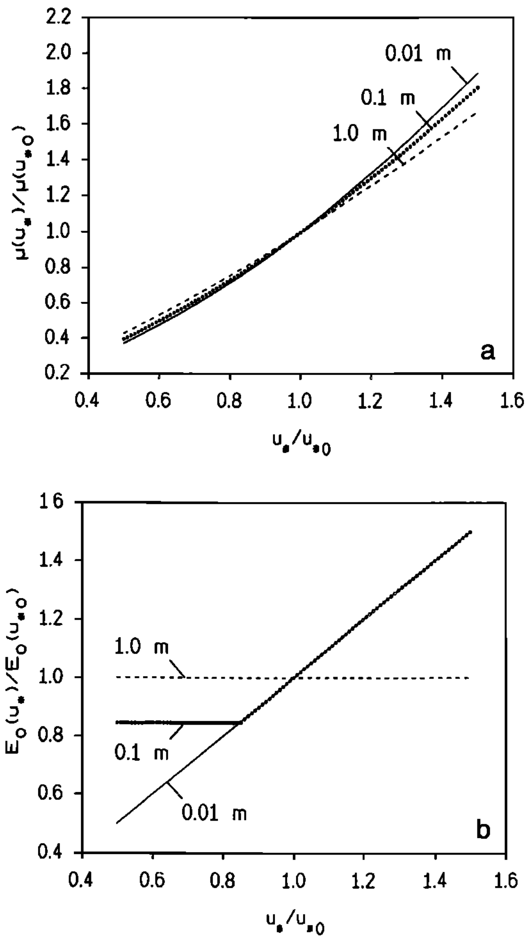

Figure 9. Relative variation of (a) the relaxation rate, μ, and (b) the equilibrium wave height spectral density, E_0, for waves with wavelengths of 0.01, 0.1, and 1.0 m, with variations of the friction velocity, u_*, around its mean value for a wind speed of 5 m/s.

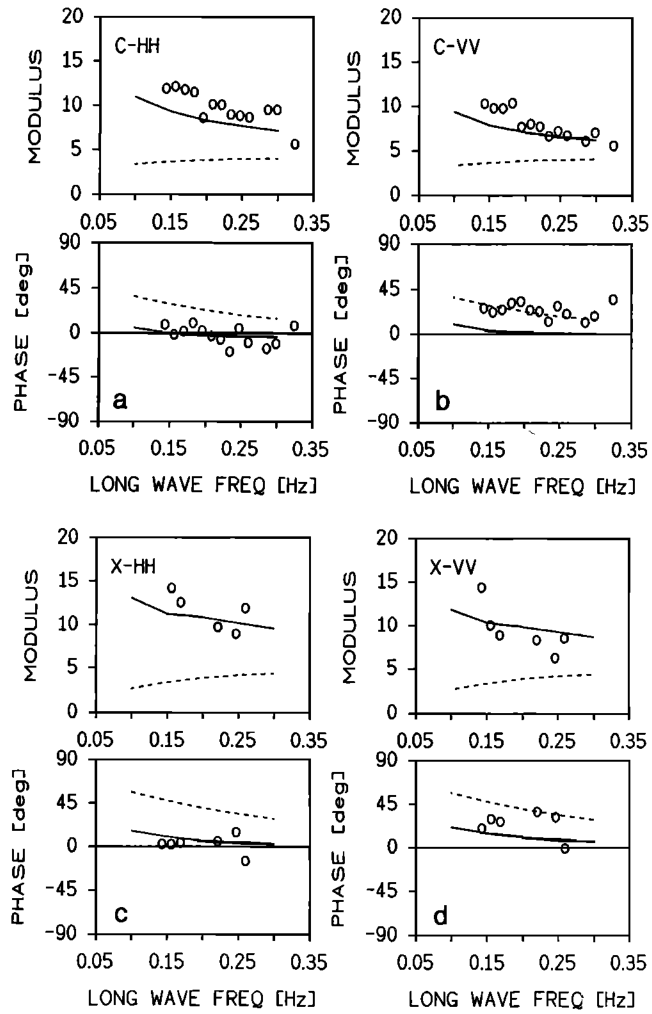

Figure 10. Same as Figure 8, but after inclusion of the best fit wind stress modulation in the three-scale model.

Our simulation results suggest that the wind stress MTF as defined by (53) depends only weakly on K, that is, that the wind stress modulation is proportional to the slope rather than to the height of the long waves. Furthermore, the phase of the wind stress modulation appears to be approximately 30° to 60° ahead of the long-wave crest, which roughly corresponds to the region of maximum surface roughness due to pure hydrodynamic modulation. This might indicate that the wind–wave modulation is associated with a positive feedback mechanism in which the local friction velocity is coupled to the local surface roughness: An increase of the surface roughness due to hydrodynamic modulation causes an increased friction velocity, which in turn results in an increased local equilibrium spectrum. The largest wind stress modulation is required in the simulations for low wind speeds. The best agreement between simulated and measured MTFs for the 5 m/s wind case is obtained if the modulus of the wind stress MTF is set to 9 and its phase to 45°. The resulting "optimized" model MTFs for C and X band are shown in Figure 10. Note that the difference between the predicted residual MTFs for HH and VV polarization becomes smaller with increasing wind stress modulation. This implies that the large measured differences cannot be explained by this modulation mechanism.

5. Discussion and Outlook

An improved three-scale composite surface model for the modulation of the backscattered radar power from the sea surface by long ocean waves has been developed. The model includes the hydrodynamic modulation of intermediate-scale waves (wavelengths between the length of the Bragg waves and the length of the long waves which are resolved by the radar) by the long waves, as well as it includes the hydrodynamic modulation of the short Bragg waves by the entire spectrum of longer waves. The long and intermediate-scale waves affect the radar backscatter by second-order geometric and hydrodynamic modulation which depends on the local mean square facet slope. It was also shown that the mean hydrodynamic modulation of the Bragg waves by the longer waves, which causes an upwave / downwave (or upwind / downwind) asymmetry of the radar backscatter, gives a significant contribution to the radar backscatter at high microwave frequencies. This contribution has not been taken into account in previous three-scale composite surface models. In addition, our numerical implementation of the proposed model allows an optional inclusion of additional modulation mechanisms such as a modulation of the wind stress over long ocean waves.

A comparison between ocean wave–radar modulation transfer functions (MTFs) obtained from the proposed model and from tower-based scatterometer measurements has been carried out. It was shown that basic features of the measured MTFs are better reproduced by the three-scale model than by conventional theory. In particular, the measured differences of the phases and magnitudes of the "hydrodynamic" or "residual" MTFs for HH and VV polarization can be explained at least qualitatively by the three-scale model, whereas the conventional model predicts no difference at all. However, while the phases obtained from the proposed model agree quite well with our experimental results, the magnitude of the "residual" MTF for high microwave frequencies still appears to be underestimated. This indicates that additional modulation mechanisms must be present.

It was demonstrated that the agreement between model results and measurements can be significantly improved by including a modulation of the wind stress over long waves in the hydrodynamic part of the proposed model. However, experimental evidence of this kind of wind stress modulation does not yet exist. Furthermore, the large measured differences between the "residual" MTFs for HH and VV polarization very likely cannot be completely explained within the framework of the proposed model.

The next step toward further improvement of the theory should be a comprehensive analysis of the model results under different environmental conditions. In particular, the dependence of the discrepancies between model predictions and experimental results on wind speed, wave height, and on the form of the wave height spectrum must be investigated in more detail. In addition, we know now that the ocean wave–radar modulation mechanism is more complex than expected from conventional theory. The backscattered radar power is affected not only by the first-order modulation of the Bragg waves but also, to a considerable extent, by variations of the entire wave spectrum. Therefore, detailed knowledge of the modulation of the short and intermediate-scale waves is required, which cannot be obtained only from the scatterometer data. High-resolution methods like stereo photography appear to be better suited for such measurements. Also, the wind stress variations over long ocean waves need to be investigated in more detail. The major question to be addressed by such experiments is whether the remaining discrepancies between model predictions and measurements of the ocean wave–radar MTF can be attributed to the hydrodynamic part or to the radar part of the existing model.

Acknowledgments. The authors thank Volkmar Wismann for designing the radar system and for numerous productive discussions. This work has been supported by the Bundesministerium für Forschung und Technologie, Bonn, under contract 01QS90160, and by the Fraunhofer-Gesellschaft, München, under contract T/RF35/L0013/L1309 (SAXON-FPN).

References

Alpers, W., and K. Hasselmann, The two-frequency microwave technique for measuring ocean wave spectra from an airplane or satellite, *Boundary Layer Meteorol.*, *13*, 215–230, 1978.

Alpers, W., and I. Hennings, A theory of the imaging mechanism of underwater bottom topography by real and synthetic aperture radar, *J. Geophys. Res.*, *89*, 10,529–10,546, 1984.

Alpers, W., and W.L. Jones, The modulation of the radar backscattering cross-section by long ocean waves, in *Proceedings of the Twelfth International Symposium on Remote Sensing of Environment*, edited by J.J. Cook, pp. 1,597–1,606, Environmental Research Institute of Michigan, Ann Arbor, 1978.

Alpers, W., D.B. Ross, and C.L. Rufenach, On the detectability of ocean surface waves by real and synthetic aperture radar, *J. Geophys. Res.*, *86*, 6,481–6,498, 1981.

Bjerkaas, A.W., and F.W. Riedel, Proposed model for the elevation spectrum of a wind-roughened sea surface, *Rep. TG-1328*, 32 pp., Appl. Phys. Lab., Johns Hopkins Univ., Laurel, Md., 1979. (Also available as *ADA083426* from Natl. Tech. Inf. Serv., Springfield, Va.)

Bretherton, F.P., Linearized theory of wave propagation, *Lect. Appl. Math.*, *13*, 61–102, 1970.

Caponi, E.A., D.R. Crawford, H.C. Yuen, and P.G. Saffman, Modulation of radar backscatter from the ocean by a variable surface current, *J. Geophys. Res.*, *93*, 12,249–12,263, 1988.

Feindt, F., Radar-Rückstreuexperimente am Wind-Wellen-Kanal bei sauberer und filmbedeckter Wasseroberfläche im X-Band (9.8 GHz), Hamburger Geophys. Einzelschrift., *Reihe A*, *75*, 234 pp., Fachbereich Geowissenschaften, Universität Hamburg, Germany, 1985.

Feindt, F., J. Schröter, and W. Alpers, Measurements of the ocean wave–radar modulation transfer function at 35 GHz from a sea-based platform in the North Sea, *J. Geophys. Res.*, *91*, 9,701–9,708, 1986.

Gower, J.F.R., "Layover" in satellite radar images of ocean waves, *J. Geophys. Res.*, *88*, 7,719–7,720, 1983.

Hara, T., and W.J. Plant, Hydrodynamic modulation of short wind-wave spectra due to long waves measured by microwave radar, *J. Geophys. Res.*, this issue.

Holliday, D., G. St-Cyr, and N.E. Woods, A radar ocean imaging model for small to moderate incidence angles, *Int. J. Remote Sens.*, *7*, 1,809–1,834, 1986.

Holliday, D., G. St-Cyr, and N.E. Woods, Comparison of a new radar ocean imaging model with SARSEX internal wave image data, *Int. J. Rem. Sens.*, *8*, 1,423–1,430, 1987.

Hughes, B.A., The effect of internal waves on surface wind waves, 2, Theoretical analysis, *J. Geophys. Res.*, *83*, 455–465, 1978.

Inoue, T., On the growth of the spectrum of a wind generated sea according to a modified Miles-Phillips mechanism and its application to wave forecasting, *Rep. TR-67-5*, Geophys. Sci. Lab., N.Y. Univ., New York, 1967.

Kasilingam, D.P., and O.H. Shemdin, The validity of the composite surface model and its applications to the modulation of radar backscatter, *Int. J. Remote Sens.*, *13*, 2,079–2,104, 1992.

Keller, W.C., and J.W. Wright, Microwave scattering and the straining of wind-generated waves, *Radio Sci.*, *10*, 139–147, 1975.

Longuet-Higgins, M.S., and R.W. Stewart, Radiation stresses in water waves, a physical discussion with applications, *Deep Sea Res.*, *11*, 529–562, 1964.

Lyzenga, D.R., and J.R. Bennett, Full-spectrum modeling of synthetic aperture radar internal wave signatures, *J. Geophys. Res.*, *93*, 12,345–12,354, 1988.

Miles, J.W., On the generation of surface waves by shear flows, 2, *J. Fluid Mech.*, *6*, 568–582, 1959.

Mitsuyasu, H., and T. Honda, Wind-induced growth of water waves, *J. Fluid Mech.*, *123*, 425–442, 1982.

Plant, W.J., A relationship between wind stress and wave slope, *J. Geophys. Res.*, *87*, 1,961–1,967, 1982.

Plant, W.J., A two-scale model of short wind-generated waves and scatterometry, *J. Geophys. Res.*, *91*, 10,735–10,749, 1986.

Plant, W.J., The modulation transfer function: Concept and applications, in *Radar Scattering from Modulated Wind Waves*, edited by G.J. Komen and W.A. Oost, pp. 173–181, Kluwer Academic, Norwell, Mass., 1989.

Plant, W.J., W.C. Keller, and J.W. Wright, Modulation of coherent microwave backscatter by shoaling waves, *J. Geophys. Res.*, *83*, 1,347–1,352, 1978.

Plant, W.J., W.C. Keller, and A. Cross, Parametric dependence of the ocean wave-radar modulation transfer function, *J. Geophys. Res.*, *88*, 9,747–9,756, 1983.

Saxton, J.A., and J.A. Lane, Electrical properties of sea water, *Wireless Eng.*, *291*, 269–275, 1952.

Schiff, L.I., *Quantum Mechanics*, McGraw-Hill, New York, 1955.

Schröter, J., F. Feindt, W. Alpers, and W.C. Keller, Measurement of the ocean wave-radar modulation transfer function at 4.3 GHz, *J. Geophys. Res.*, *91*, 923–932, 1986.

Smith, J.A., Modulation of short wind waves by long waves, in *Surface Waves and Fluxes*, Vol. 1, *Current Theory*, edited by G.L. Geernaert and W.J. Plant, pp. 247–284, Kluwer Academic, Norwell, Mass., 1990.

Snyder, R.L., and C.S. Cox, A field study of the wind generation of ocean waves, *J. Mar. Res.*, *24*, 141–178, 1966.

Snyder, R.L., F.W. Dobson, J.A. Elliott, and R.B. Long, Array measurements of atmospheric pressure fluctuations above surface gravity waves, *J. Fluid Mech.*, *102*, 1–59, 1981.

Stolte, S., Modulation des kurzwelligen Seegangs durch langwelligen Seegang und Wind, *Dissertation zur Erlangung des Doktorgrades*, 119 pp., Fachbereich Geowissenschaften, Universität Hamburg, Germany, 1984.

Stolte, S., Measurements of ocean short scale roughness, in IGARSS '91, Remote Sensing: Global Monitoring for Earth Management, *IEEE Publ. 91CH2971-0*, pp. 2,005–2,008, Inst. of Elec. and Electron. Eng., New York, 1991.

Stratton, J.A., *Electromagnetic Theory*, McGraw-Hill, New York, 1941.

Thompson, D.R., Calculation of microwave Doppler spectra from the ocean surface with a time-dependent composite model, in *Radar Scattering from Modulated Wind Waves*, edited by G.J. Komen and W.A. Oost, pp. 27–40, Kluwer Academic, Norwell, Mass., 1989.

Thompson, D.R., Intensity modulations in synthetic aperture radar images of ocean surface currents and the wave / current interaction process, *Johns Hopkins APL Tech. Dig.*, *6*, 346–353, 1990.

Thompson, D.R., and R.F. Gasparovic, Intensity modulation in SAR images of internal waves, *Nature*, *320*, 345–348, 1986.

Thompson, D.R., B.L. Gotwols, and W.C. Keller, A comparison of K_u band Doppler measurements at 20° incidence with predictions from a time-dependent scattering model, *J. Geophys. Res.*, *96*, 4,947–4,955, 1991.

Valenzuela, G.R., Theories for the interaction of electromagnetic and ocean waves: A review, *Boundary Layer Meteorol.*, *13*, 61–85, 1978.

Whitham, G.B., A general approach to linear and non-linear dispersive waves using a Lagrangian, *J. Fluid Mech.*, *22*, 273–283, 1965.

Willebrand, J., Energy transport in a nonlinear and inhomogeneous random gravity wave field, *J. Fluid Mech.*, *70*, 113–126, 1975.

Wright, J.W., A new model of sea clutter, *IEEE Trans. Antennas Propag.*, *AP-16*, 217–223, 1968.

Wright, J.W., Detection of ocean waves by microwave radar: The short gravity-capillary waves, *Boundary Layer Meteorol.*, *13*, 101–102, 1978.

Wright, J.W., W.J. Plant, W.C. Keller, and W.L. Jones, Ocean wave-radar modulation transfer functions from the West Coast Experiment, *J. Geophys. Res.*, *85*, 4,957–4,966, 1980.

W. Alpers, R. Romeiser, and A. Schmidt, Institut für Meereskunde, Universität Hamburg, Troplowitzstr. 7, 22529 Hamburg, Federal Republic of Germany.

(Received April 5, 1993; revised November 30, 1993; accepted November 30, 1993.)